JOURNAL OF GEOPHYSICAL RESEARCH, VOL. 100, NO. B2, PAGES 2123–2133, FEBRUARY 10, 1995

Numerical simulation of elastic wave propagation using a finite volume method

Emmanuel Dormy and Albert Tarantola

Département de Sismologie, Institut de Physique du Globe de Paris, Paris, France

Abstract. Like the finite difference method, the finite volume method gives an approximate value for the derivative of a field at a given point using the values of the field at a few locations neighboring the point. The method uses the divergence theorem, considers a "finite volume" around the point and discretizes the surface bounding the volume. When the finite volumes considered are regular polyhedra, one obtains the expressions corresponding to standard centered finite differences, but the finite volume method is more general than the finite difference method because it may deal directly with irregular grids. It is possible to give a finite volume formulation of the elastodynamic problem, using dual volumes, that correspond, in the regular case, to the staggered grids used in the finite difference method. The scheme thus obtained is more general than the one obtained using finite differences, as the "grids" may be totally unstructured, but at the cost of having, in the general case, only a first-order accuracy. Although the scheme is not consistent, numerical tests suggest that it is stable and convergent. This implementation of a finite volume method does not provide a way for a more general treatment of the boundaries than the conventional finite difference method.

Introduction

Finite differences have proved their usefulness in solving differential equation problems and, in particular, in modeling the propagation of elastic waves [*Kelly et al.*, 1976; *Virieux*, 1986], but the fact that they are implemented using regular grids gives rise to several numerical problems, including numerical anisotropy associated with the anisotropy of the grid. As an alternative to the finite difference method, one can use a finite element method or a finite volume method. If finite element methods have already been used to simulate wave propagation [e.g., *Marfurt*, 1984], the only example we know of using a finite volume method in a dynamical problem was made by *Hermeline* [1993] and concerned Maxwell's equations.

Preliminary results concerning the finite volume method have been obtained by T. Gallouët (manuscript in preparation 1992) and *Faille et al.* [1991]. We here depart from the method as proposed by the previous authors, where the differential equation considered is a conservation equation. In this paper we use the finite volume method as a general method for numerical estimation of derivatives.

Paper number 94JB02648.
0148-0227/95/94JB-02648$05.00

A Finite Volume Method

Definitions

In what follows, we assume a Euclidean space furnished with Cartesian coordinates. We put all tensor indices in the subscript position and assume the summation convention for repeated indices.

The finite volume method is based on the divergence theorem, stating that the volume integral of the divergence of a vector field w_i equals the flux of the field:

$$\int_{\mathcal{V}} dV\, \partial_i w_i = \int_{\mathcal{S}} dS\, n_i\, w_i\,. \tag{1}$$

Here, $\mathcal{S}$ is the boundary of the volume $\mathcal{V}$, and n_i is the (unitary) normal to the surface, pointing outwards.

In Euclidean spaces with Cartesian coordinates, this equation is easily generalized to the gradient of an arbitrary tensor field:

$$\int_{\mathcal{V}} dV\, \partial_i W_{jk\ldots} = \int_{\mathcal{S}} dS\, n_i\, W_{jk\ldots}\,. \tag{2}$$

In two dimensions,

$$\int_{\mathcal{S}} dS\, \partial_i W_{jk\ldots} = \int_{\mathcal{L}} dL\, n_i\, W_{jk\ldots}\,, \tag{3}$$

where $\mathcal{L}$ is the boundary of the surface $\mathcal{S}$.

The question is, How can we approximate the gradient of a tensor field at a point $\mathcal{P}$ given the values of the field at some points $\{\mathcal{P}^\alpha\} = \{\mathcal{P}^1, \mathcal{P}^2, \ldots\}$ around $\mathcal{P}$? The problem is illustrated by Figure 1.

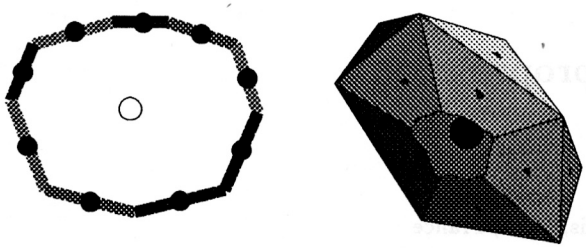

$$\partial_i V_{jk\ldots} \approx \frac{1}{\Delta S} \sum_\alpha \Delta L^\alpha \, n_i^\alpha \, V_{jk\ldots}^\alpha \qquad \partial_i V_{jk\ldots} \approx \frac{1}{\Delta V} \sum_\alpha \Delta S^\alpha \, n_i^\alpha \, V_{jk\ldots}^\alpha$$

Figure 1. We wish to approximately estimate the gradient of a tensor field at a point $\mathcal{P}$ given the values of the field at some points $\{\mathcal{P}^\alpha\} = \{\mathcal{P}^1, \mathcal{P}^2, \ldots\}$ around $\mathcal{P}$. (left) In 2-D, the points $\{\mathcal{P}^\alpha\}$ are used to define a polygon surrounding the point $\mathcal{P}$. Then a discretization of the (Gauss) divergence theorem (see text) gives the approximation $\partial_i V_{jk\ldots} \approx \frac{1}{\Delta S} \sum_\alpha \Delta L^\alpha \, n_i^\alpha \, V_{jk\ldots}^\alpha$, where ΔS is the surface inside the polygon, ΔL^α and n_i^α are respectively the length and unit normal to the αth side of the polygon, and $V_{jk\ldots}^\alpha$ is the value of the tensor field at a point on this side. (right) In 3-D, the points $\{\mathcal{P}^\alpha\}$ are used to define a polyhedron surrounding the point $\mathcal{P}$. Then a discretization of the (Gauss) divergence theorem (see text) gives the approximation $\partial_i V_{jk\ldots} \approx \frac{1}{\Delta V} \sum_\alpha \Delta S^\alpha \, n_i^\alpha \, V_{jk\ldots}^\alpha$, where ΔV is the volume inside the polyhedron, ΔS^α and n_i^α are respectively the surface and unit normal to the αth facet of the polyhedron, and $V_{jk\ldots}^\alpha$ is the value of the tensor field at a point on this facet.

In the two-dimensional (2-D) case, discretizing the boundary of the surface $\mathcal{S}$ by some segments with length $\{\Delta L^\alpha\} = \{\Delta L^1, \Delta L^2, \ldots\}$ and outward (unit) normal $\{n_i^\alpha\} = \{n_i^1, n_i^2, \ldots\}$, where the tensor field takes the values $\{V_{ij\ldots}^\alpha\} = \{V_{ij\ldots}^1, V_{ij\ldots}^2, \ldots\}$, the divergence theorem (3) gives, with a smooth enough $\partial_i V_{jk\ldots}$,

$$\Delta S \, \partial_i V_{jk\ldots} \approx \sum_\alpha \Delta L^\alpha \, n_i^\alpha \, V_{jk\ldots}^\alpha \,, \tag{4}$$

i.e.,

$$\partial_i V_{jk\ldots} \approx \frac{1}{\Delta S} \sum_\alpha \Delta L^\alpha \, n_i^\alpha \, V_{jk\ldots}^\alpha \,. \tag{5}$$

In the three-dimensional (3-D) case, discretizing the boundary of the volume $\mathcal{V}$ by some facets with surface $\{\Delta S^\alpha\} = \{\Delta S^1, \Delta S^2, \ldots\}$ and outward (unit) normal $\{n_i^\alpha\} = \{n_i^1, n_i^2, \ldots\}$, where the tensor field takes the values $\{V_{ij\ldots}^\alpha\} = \{V_{ij\ldots}^1, V_{ij\ldots}^2, \ldots\}$, the divergence theorem (2) gives

$$\Delta V \, \partial_i V_{jk\ldots} \approx \sum_\alpha \Delta S^\alpha \, n_i^\alpha \, V_{jk\ldots}^\alpha \,, \tag{6}$$

i.e.,

$$\partial_i V_{jk\ldots} \approx \frac{1}{\Delta V} \sum_\alpha \Delta S^\alpha \, n_i^\alpha \, V_{jk\ldots}^\alpha \,. \tag{7}$$

Equations (5) and (7) give the finite volume approximation to the gradient of a tensor field in the 2-D case and in the 3-D case, respectively.

Application to Regular Grids in 2-D and 3-D

Two-Dimensional Cartesian Grid. When in a two-dimensional space, a lozenge (or a square) is considered, the application of formula (5) gives (see Figure 2)

$$\partial_x V_{ij\ldots}(\mathcal{O}) \approx \frac{V_{ij\ldots}(\mathcal{B}) - V_{ij\ldots}(\mathcal{A})}{2\,\Delta x} \,, \tag{8}$$

and

$$\partial_y V_{ij\ldots}(\mathcal{O}) \approx \frac{V_{ij\ldots}(\mathcal{D}) - V_{ij\ldots}(\mathcal{C})}{2\,\Delta y} \,, \tag{9}$$

which correspond to standard finite difference expressions for centered derivatives. Here, $2\,\Delta x$ and $2\,\Delta y$ correspond to the lengths of the diagonals of the lozenge. Appendix A.1 contains an explicit demonstration of the formulas.

Figure 3 shows the plane paved with rhombuses (or squares). The set of solid and open points corresponds to the standard grids used in centered staggered finite difference approximations. When choosing lozenges to pave the plane, there is a complete equivalence between the finite volume and the finite difference method. The advantage of the finite volume method is that the grid can be perturbed and, thus, become irregular (see the numerical examples below).

Two-Dimensional Minimal Grid. To estimate derivatives, centered finite difference methods use two points along each space dimension. This makes $2N$ points in a space of dimension N : four points in 2-D and six points in 3-D. But a centered finite difference approximation to derivatives can be obtained using only $N+1$ points, i.e., three points in 2-D and four points in 3-D, as shown by *Magnier et al.* [1994], who simulated the propagation of elastic waves in 2-D. A grid using only $N+1$ points to estimate derivatives was called by the authors a "minimal grid."

Let us show that, from the viewpoint of this work, a minimal grid in 2-D corresponds to the paving of the plane with hexagons.

Application of formula (5) to a regular hexagonal cell gives (see Figure 4)

$$(\partial_x V_{ij\ldots})(\mathcal{O}) \approx \frac{V_{ij\ldots}(\mathcal{B}) - V_{ij\ldots}(\mathcal{A})}{2\,\Delta} \,, \tag{10}$$

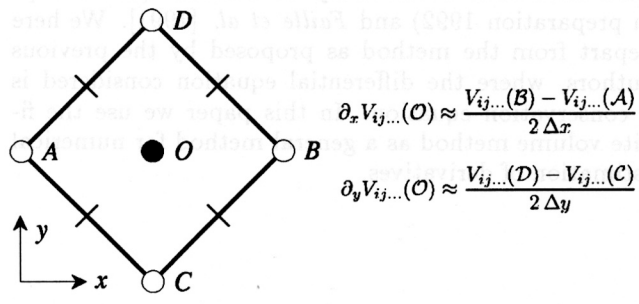

Figure 2. When, in 2-D, the finite volume (in fact, finite surface) is a lozenge, the approximation obtained for the derivative is exactly that given by standard (centered) finite differences (see text). The values $2\,\Delta x$ and $2\,\Delta y$ correspond to the lengths of the diagonals of the lozenge.

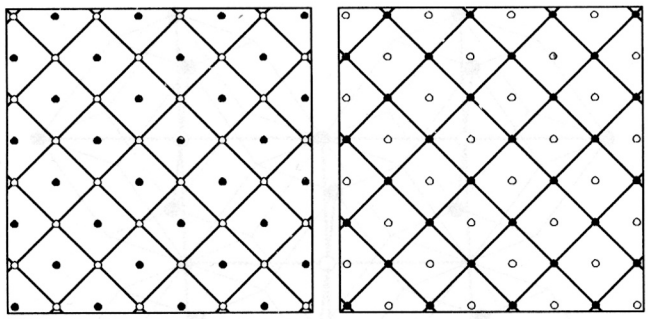

Figure 3. A 2-D Euclidean space may be filled with contiguous lozenges. The formulas then obtained with the finite volume method are identical to those obtained using finite differences in staggered grids. If the figure at left gives the first derivatives of a tensor field at solid points using the values of the tensor field at the open points, the finite volumes (in fact, surfaces) outlined at right give at open points the second derivatives of the tensor field using the values of the first derivatives known at the solid point. The lines represented here represent the surfaces used for computation, but the same grid is usually represented with vertical and horizontal lines.

and

$$(\partial_y V_{ij\ldots})(\mathcal{O}) \approx \frac{V_{ij\ldots}(\mathcal{C}) - \frac{1}{2}(V_{ij\ldots}(\mathcal{B}) + V_{ij\ldots}(\mathcal{A}))}{\sqrt{3}\,\Delta}\,, \tag{11}$$

which corresponds to the expressions given by *Magnier et al.* [1994] for their minimal grids. Appendix B.1 contains an explicit demonstration of the formulas.

Figure 5 shows the plane paved with hexagons. The set of solid and open points corresponds to the minimal grids, where, in 2-D, each point is surrounded by three other points.

Three-Dimensional Cartesian Grid. The 3-D Cartesian grid, used for centered finite difference computations, is quite simple: each point where the partial derivatives of a field are sought is surrounded by six other points (right-left, front-back and top-bottom). This simple structure is similar to that of a crystal of NaCl, where each atom of Cl is surrounded by six atoms of Na (and vice versa). It is represented in Figure 6.

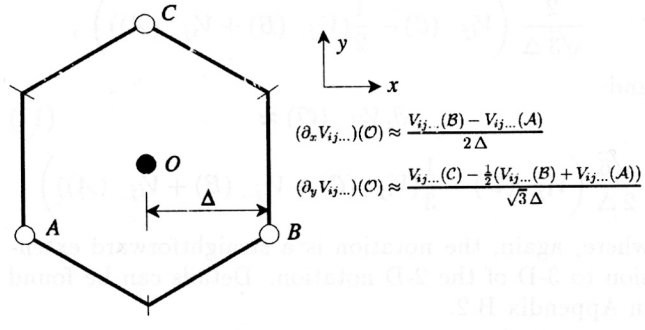

Figure 4. We use here a cell which allows one to compute a gradient using a minimal number of points (one more point than the dimension of the space). In the 1-D case only two points are needed to define a linear function and approximate a gradient. In 2-D as shown here, three points are required.

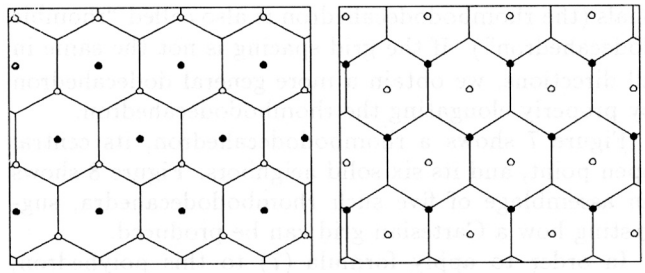

Figure 5. A 2-D Euclidiean space may be filled with contiguous hexagons. The way those two grids are used to compute the second derivative of a tensor field is basically the same as in the Cartesian case. While the finite "volumes" outlined on the left part of the figure give the derivative at the solid points, the ones outlined on the right give the derivative at the open points.

To interpret this Cartesian grid within the finite volume context, we need to solve the following problem: how can the 3-D space be partitioned into identical polyhedra such that the centers of the polyhedra correspond to the open (or solid, respectively) points in Figure 6?

In other words, if the Cl atoms (or the Na atoms, respectively) in a crystal of ClNa are "inflated" they will be spherical until they eventually come into contact. If they are inpenetrable and if they continue to be inflated until all the space between them is filled, which polyhedron will be obtained? The polyhedron thus defined (the part of the space whose points are closer to a given point than to any other point) has different names in different contexts. Crystallographers call this the Wigner-Seitz cell [*Kittel*, 1966] and mathematicians, the Voronoï cell [*Edelsbrunner*, 1987]. In 2-D, this problem has been solved above. The square and the hexagon are the Voronoï cells for the 2-D Cartesian grid and 2-D minimal grid, respectively.

What about the 3-D Cartesian grid? If the grid spacing is the same in all space dimensions, the figure obtained when inflating the white points in Figure 6 is a rhombododecahedron, i.e., a polyhedron with 12 identical faces: lozenges with a $\sqrt{2}$ ratio between their diag-

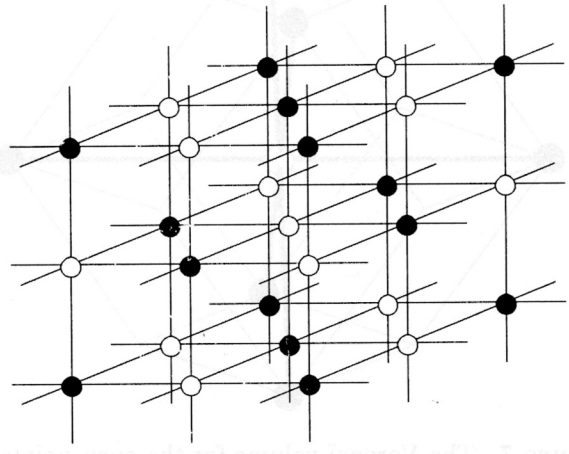

Figure 6. The 3-D Cartesian grid used in the finite difference method.

onals (the rhombododecahedron is also called "rhombic dodecahedron"). If the grid spacing is not the same in all directions, we obtain a more general dodecahedron by properly elongating the rhombododecahedron.

Figure 7 shows a rhombododecahedron, its central open point, and its six solid neighbors. Figure 8 shows an assemblage of five such rhombododecahedra, suggesting how a Cartesian grid can be produced.

In order to apply formula (7) to this polyhedron, where six values of the function to be differentiated are defined, we assume that the value of the field on the four half-faces of the rhombododecahedron is equal to that at the common node (see, for instance, Figure 14). We then obtain the same formulas as the ordinary centered finite difference method:

$$\partial_x V_{ij\ldots}(\mathcal{O}) \approx \frac{V_{ij\ldots}(\mathcal{B}) - V_{ij\ldots}(\mathcal{A})}{2\,\Delta x}\,, \tag{12}$$

$$\partial_y V_{ij\ldots}(\mathcal{O}) \approx \frac{V_{ij\ldots}(\mathcal{D}) - V_{ij\ldots}(\mathcal{C})}{2\,\Delta y}\,, \tag{13}$$

and

$$\partial_z V_{ij\ldots}(\mathcal{O}) \approx \frac{V_{ij\ldots}(\mathcal{F}) - V_{ij\ldots}(\mathcal{E})}{2\,\Delta z}\,, \tag{14}$$

where the notation is a straightforward extension of that used in the 2-D case. Details are provided in Appendix A.2.

Intersecting the rhombododecahedral mesh by one of the three principal symmetry planes gives rise to the lozenge considered in 2-D.

Three-Dimensional Minimal Grid. To compute finite differences in 3-D using a minimal grid, we need four points defining a tetrahedron, surrounding the central point (Figure 9).

We need to determine the paving of the space which corresponds, within the finite volume context, to this minimal grid. In other words, which Voronoï polyhedron is associated with the open (or solid) points of the grid shown in Figure 9?

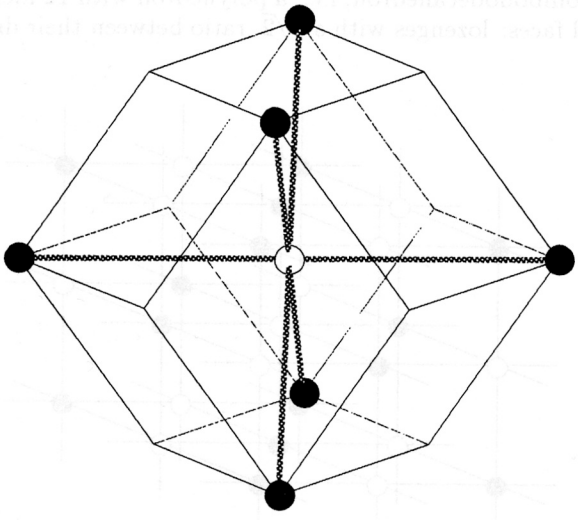

Figure 7. The Voronoï volume for the open points in Figure 6 is a rhombododecahedron.

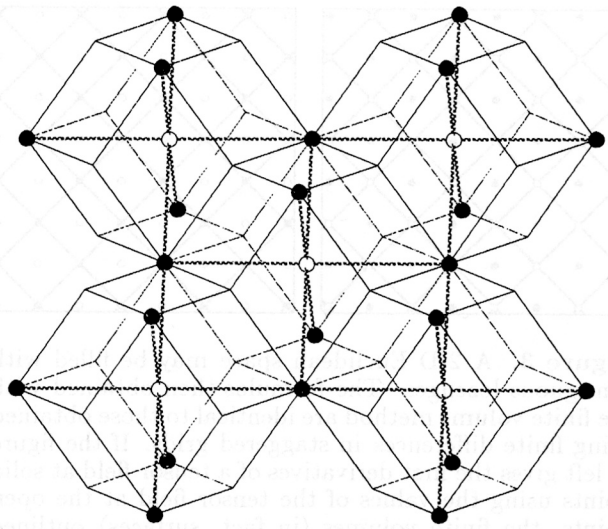

Figure 8. Paving the space with rhombododecahedra like the one shown in Figure 7 leads to the 3-D Cartesian grid used in finite difference computations.

Surprising as this may seem at first glance, the answer is the same as for the Cartesian grid: the rhombododecahedron. Figure 10 shows the same assemblage of five rhombododecahedra as Figure 8, but here the central point is not connected to those vertices having four facets, but rather to four of the vertices having three facets (there are two such possibilities). We thus see that the same tessellation of the space by rhombododecahedra produces, depending on the vertices we select to join to the central point, either a Cartesian grid or a minimal grid.

The application of formula (7) to this polyhedron, and with this selection of nodes and facets (i.e., four values, each one associated with three faces, as illustrated in Figure 14), gives, for the finite volume method, the same formulas as those obtained by *Magnier et al.* [1994] for the minimal grid, finite difference method:

$$\partial_x V_{ij\ldots}(\mathcal{O}) \approx \frac{V_{ij\ldots}(\mathcal{B}) - V_{ij\ldots}(\mathcal{A})}{\Delta}\,, \tag{15}$$

$$\partial_y V_{ij\ldots}(\mathcal{O}) \approx \tag{16}$$

$$\frac{2}{\sqrt{3}\,\Delta}\left(V_{ij\ldots}(\mathcal{C}) - \frac{1}{2}(V_{ij\ldots}(\mathcal{B}) + V_{ij\ldots}(\mathcal{A}))\right)\,,$$

and

$$\partial_z V_{ij\ldots}(\mathcal{O}) \approx \tag{17}$$

$$\frac{\sqrt{6}}{2\,\Delta}\left(V_{ij\ldots}(\mathcal{D}) - \frac{1}{3}(V_{ij\ldots}(\mathcal{C}) + V_{ij\ldots}(\mathcal{B}) + V_{ij\ldots}(\mathcal{A}))\right)\,,$$

where, again, the notation is a straightforward extension to 3-D of the 2-D notation. Details can be found in Appendix B.2.

Pseudoconsistency of the Finite Volume Method

We have just shown that when the space is paved with polyhedra that have the necessary symmetries, the fi-

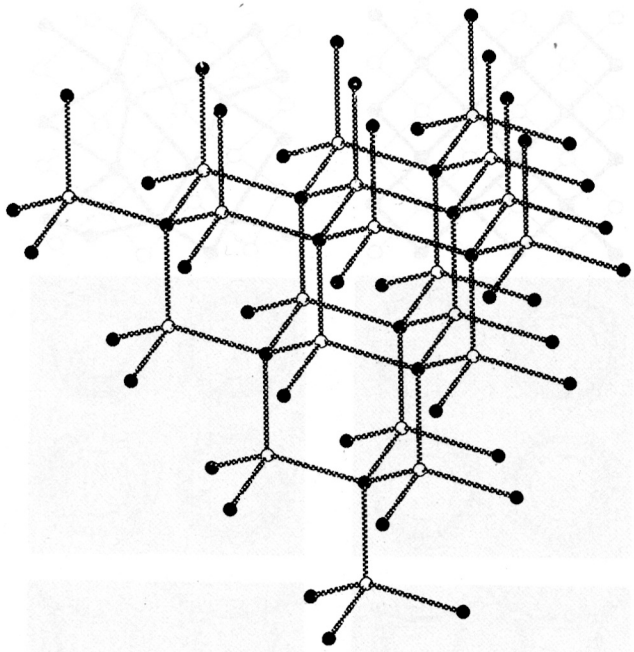

Figure 9. The 3-D minimal grid. To estimate derivatives in 3-D at a given point, only four neighboring points are needed. In this grid, each open point has four solid neighbors, and each solid point has four open neighbors. This was called a "minimal grid" by *Magnier et al.* [1994].

nite volume method gives the same approximation to first-order derivatives as the finite difference method. The interest of the finite volume method is that it can be used with nonstructured grids, as the polyhedra with which we pave the space may be irregular, or even have a variable number of faces. Needless to say, the approximation, then, is only first order.

The consistency error of a discrete numerical scheme is defined as the error of the estimation in the limit when the discretization step tends to zero. The (centered) finite difference method, for instance, is consistent, which means that the numerical finite difference value at any point of the grid tends to the actual derivative of the function at this point, when the grid tends to be infinitely dense.

In the finite volume method described here, if the polyhedron used to estimate the gradient of a field at a given point of the space has no particular symmetry, the consistency error does not tend to zero when the size of the polyhedron tends to zero: the method is not consistent. But since the polyhedra need to pave the space (leaving no holes), errors in contiguous polyhedra have, roughly speaking, opposite sign and tend, in average, to vanish. This leads to the notion of weak consistency, or pseudoconsistency.

Although the scheme we propose is not consistent, our numerical tests suggest that it is convergent, as the examples below show. It should be noted that the Lax theorem [*Lax and Richtmyer,* 1956] states that, under the consistency assumption, stability and convergence of a finite difference algorithm are equivalent properties. Here, we do not have consistency, and we limit ourselves to numerically observing both stability (if the space boundaries are properly handled and the time step is sufficiently small) and convergence.

The stability conditions found for other finite volume schemes depend, in some way, on the minimal distance between points in the grid [*Hermeline,* 1993; also T.Gallouët, manuscript in preparation, 1992]. In order to minimize the computation effort we have attempted, in our numerical experiments, to define grids that, although irregular, never have two points extremely close.

One of the motivations of this study was to understand in which way a finite volume formulation could better handle irregular boundaries. One should notice that the finite difference method, when using staggered grids, is second order only when computing derivatives "inside" the medium, but gives only a first-order approximation to the boundary conditions, where the staggering of the grid does not allow an easy description of a flat surface.

As the finite volume method reduces to the finite difference method when choosing regular polyhedra, it soon became apparent that this method, at least as here implemented, can not help in better handling the boundary conditions.

In the numerical examples below, the implementation of the boundary conditions has been circumvented in the Cartesian grids by using periodic boundary conditions. In the hexagonal grids, we have implemented both Neumann and Dirichlet boundary conditions (i.e., "rigid" and "free" surfaces), but the grid was kept regular at the boundaries (then, the finite volume implementation is totally equivalent to the minimal finite difference grids of *Magnier et al.* [1994]).

Propagation of Elastic Waves

The physics of an elastic wave propagation through a medium characterized by a mass density ρ and an

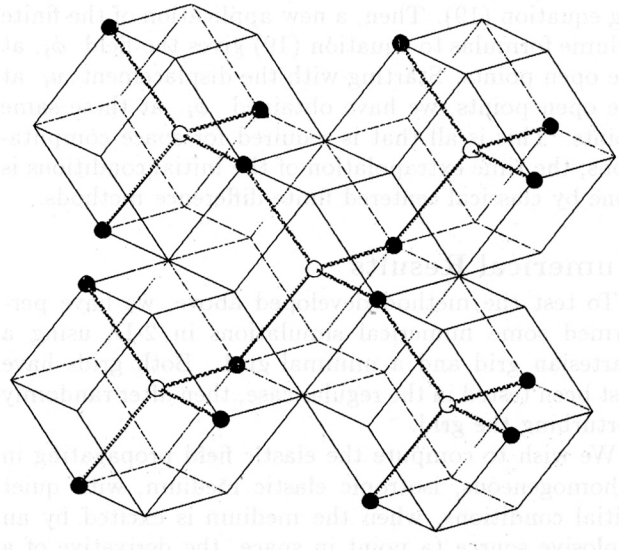

Figure 10. As for the Cartesian grid, the Voronoï polyhedron associated with the 3-D minimal grid is the rhombododecahedron.

elastic stiffness $c_{ijk\ell}$ can be completely described, using Cartesian coordinates, by the relations

$$\varepsilon_{ij} = \frac{1}{2}(\partial_i u_j + \partial_j u_i) \quad (18)$$

$$\sigma_{ij} = c_{ijk\ell}\,\varepsilon_{k\ell} + M_{ij} \quad (19)$$

$$\phi_i = \partial_j \sigma_{ij} \quad (20)$$

$$\frac{\partial v_i}{\partial t} = \frac{1}{\rho}(\phi_i + \Phi_i) \quad (21)$$

$$\frac{\partial u_i}{\partial t} = v_i\,. \quad (22)$$

Equation (18) defines the strain ε_{ij} as a function of the displacement u_i. Equation (19) gives the total stress σ_{ij} as the elastic stress (Hooke's law) plus a possible source term M_{ij}. The coefficients $c_{ijk\ell}$ define the elastic stiffness of the solid. Equation (20) defines ϕ_i, the divergence of the stress. Equation (21) corresponds to the conservation of linear momentum (when mass density is time invariant): when transposing the mass density ρ to the left-hand side it says that the inertial force density (mass density times the time derivative of the velocity v_i) equals the imposed force density (divergence of stress ϕ_i plus a possible source term Φ_i). Finally, equation (22) defines the velocity as a function of the displacement. Time extrapolation using classical centered finite differences can be found elsewhere [*Kelly et al.*, 1976; *Virieux*, 1986]. We focus on equations (18) to (20) above.

We use two dual lattices, such as those shown in Figures 3 and 5 for the regular case (more realistic examples of dual lattices, in the irregular case, are displayed at the top of Figures 11 and 12). If, for instance, the field u_i is known, at a given time, at the open points of the grid, the application of the finite volume formulas to equation (18) gives the deformation ε_{ij} at the solid points. If, at these solid points, the elastic stiffness $c_{ijk\ell}$ and the source term M_{ij} are known, the stress σ_{ij} can also be obtained at the solid points, using equation (19). Then, a new application of the finite volume formulas to equation (19) gives the field ϕ_i at the open points. Starting with the displacement u_i at the open points, we have obtained ϕ_i at these same points. This is all that is required for space computations; the time extrapolation of the initial conditions is done by classical centered finite difference methods.

Numerical Results

To test the method developed above, we have performed some numerical simulations in 2-D, using a Cartesian grid and a minimal grid. Both grids have first been tested in the regular case, then after randomly perturbing the grid.

We wish to compute the elastic field propagating in a homogeneous, isotropic elastic medium, with quiet initial conditions, when the medium is excited by an explosive source (a point in space, the derivative of a Gaussian in time).

The stiffness tensor $c_{ijk\ell}$ may contain up to 21 independent parameters in the three dimensional case, but

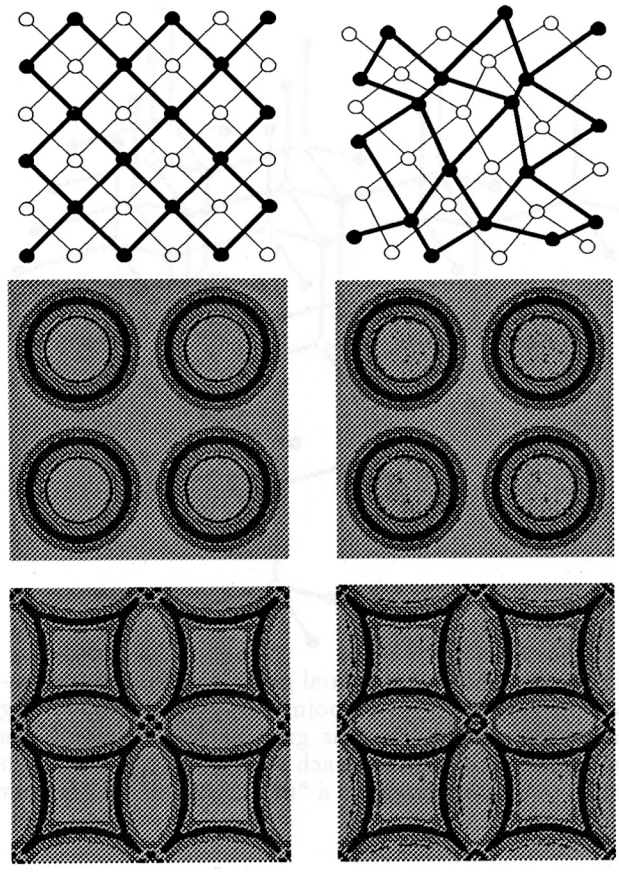

Figure 11. Numerical simulation of the propagation of elastic waves, using the finite volume method in a Cartesian grid. On the left-hand side, the grid is regular and, then, the method is equivalent to the finite difference method. On the right-hand side the grid has been randomly perturbed except for a rank of cells on the border. The top of the figure shows a detail of the grids (the full grid has 256×256 points). The middle and bottom of the figure show two snapshots of the simulation at two different time steps(the boundary conditions being periodical, two periods are shown per each dimension). The variable represented is the trace of the strain tensor ε_{ii}. The gray code used has been chosen to emphasize small values, in order to clearly display the numerical artifacts. It is interesting to note that, even for strongly perturbed grids, the numerical artifacts are surprisingly small.

for a homogeneous isotropic medium, two parameters λ and μ (Lamé's parameters) are enough to determine the elastic tensor:

$$c_{ijk\ell} = \lambda\,\delta_{ij}\delta_{k\ell} + \mu\,(\delta_{ik}\delta_{j\ell} + \delta_{i\ell}\delta_{jk})\,. \quad (23)$$

From this equation and Hooke's law (19), it follows, in the isotropic case that

$$\sigma_{ij} = \lambda\,\delta_{ij}\,\varepsilon_{kk} + 2\,\mu\,\varepsilon_{ij}\,. \quad (24)$$

The corresponding algorithm has been easily implemented on a parallel computer (Connection Machine CM-5). We need more arrays than when using a conventional finite difference method, but the codes can be parallelized with high efficiency.

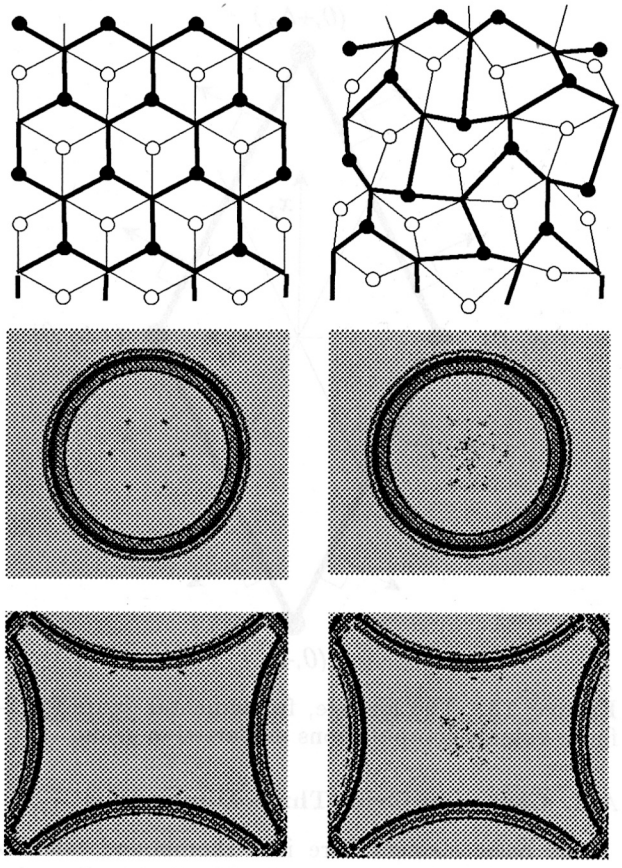

Figure 12. Numerical simulation of the propagation of elastic waves, using the finite volume method in a minimal grid. On the left-hand side, the grid is regular and, then, the method is equivalent to the finite difference method in a minimal grid. On the right-hand side the grid has been randomly perturbed except for a rank of cells on the border. The top of the figure shows a detail of the grids (the full grid has 512×512 points). The middle and bottom of the figure show two snapshots of the simulation at two different time steps. The top is a free surface (Neumann type), while the bottom and the sides are rigid (Dirichlet type). The variable represented is the trace of the strain tensor ε_{ii}. The gray code used has been chosen to emphasize small values, in order to clearly display the numerical artifacts. Even for strongly perturbed grids, the numerical artifacts are surprisingly small.

Cartesian Grid

The top row of Figure 11 shows a detail of the Cartesian grids being used. At left, the original grid and, at right, a blowup of the grid after random perturbation of the points. In both cases, periodic boundary conditions were imposed.

When modeling a second-order differential equation, like the elastic wave equation, we generally need a grid with two sorts of points: points where all the components of the displacement are given and points where all the components of the stress are given. This is, for instance, true for a minimal grid (see example below).

In the very special case where a regular Cartesian grid is used, we have a phenomenon of grid splitting: the general grid with only two sorts of points splits into two independent grids with four sorts of points: points where the displacement u_x is given, points where the displacement u_y is given, points where the stress σ_{xy} is given and, finally points where the two stresses σ_{xx} and σ_{yy} are given (see *Virieux* [1986] for an example).

This, of course, also happens when we use the regular grid at the left of Figure 11. But when the grid is perturbed (right of the figure), there is no grid splitting, and the two familiar grids are coupled. The problem is that the two grids are only weakly coupled if the perturbation of the regularity of the grid is small. To suppress any possible numerical difficulty with weakly coupled grids, we choose here a source function which, in addition to being smooth in time, is also smooth in space (Gaussian spreading on approximately 10 grid points per direction, and derivative of a Gaussian in time).

The middle and bottom rows of Figure 11 show the numerical results of the simulation. The boundary conditions being periodical, we choose to show two periods per each dimension. In the first snapshot, the wave has not yet arrived at the boundary, while in the second snapshot, the wave is already interfering with its image arriving from the boundary.

The variable represented is the dilatation (i.e., the trace of the strain tensor ε_{ii}). The gray scale used in the display has been chosen to accentuate small values, in order to clearly display the numerical artifacts. It is interesting to note that, even for strongly perturbed grids, the numerical artifacts are quite small.

Minimal Grid

As already mentioned, there is no phenomenon of grid splitting in this case. We have thus chosen a source that acts only on one point of the grid (and is smooth in time). The grid used is shown in the top row of Figure 12. Here, we have implemented free boundary conditions at the top of the medium, and rigid boundary conditions at the bottom and the two sides. The left of Figure 12 shows the results obtained for a regular grid (in this case, the finite volume method is equivalent to the finite difference method with minimal grids). When randomly perturbing the grid, we obtain the results shown at the right of the figure. Here we have perturbed all the points of the grid except the points at the boundary.

Conclusion

The finite volume method provides an alternative to the finite difference method. Being directly based on the divergence theorem, it is easier to understand theoretically. Contrary to the finite difference method, the finite volume method allows one to consider unstructured grids (we have tested only numerically perturbing structured grids).

The numerical scheme is more general than the one obtained using finite differences, as the grids may be totally unstructured, but at the cost of having, in the

general case, only a first-order accuracy. Although the scheme is not consistent, the numerical tests have shown that it is stable and convergent.

The numerical artifacts obtained when strongly perturbing regular Cartesian grids or minimal grids are quite small.

A potential possibility of this method is that a totally unstructured grid would, by definition, be totally isotropic.

Implementation of boundary conditions and convergence properties deserve further study.

Appendix A: Formulas for Regular Cartesian Grids

A.1. Cartesian Grid, Two Dimensions

The basic element here is a lozenge. If the grid spacings are Δ_1 and Δ_2 (see Figure 13), we have the following: The coordinates of the vertices are

$$\begin{aligned} P_1 &= (-\Delta_1, 0), \\ P_2 &= (+\Delta_1, 0), \\ P_3 &= (0, -\Delta_2), \\ P_4 &= (0, +\Delta_2). \end{aligned} \tag{A1}$$

The length of the sides is given by

$$\ell = \sqrt{\Delta_1^2 + \Delta_2^2}. \tag{A2}$$

The surface is given by

$$S = 2\,\Delta_1\,\Delta_2. \tag{A3}$$

The normals are

$$\begin{aligned} n_{2,4} &= \tfrac{1}{\ell}\begin{pmatrix} +\Delta_2 \\ +\Delta_1 \end{pmatrix} \quad ; \quad n_{4,1} = \tfrac{1}{\ell}\begin{pmatrix} -\Delta_2 \\ +\Delta_1 \end{pmatrix} ; \\ n_{1,3} &= \tfrac{1}{\ell}\begin{pmatrix} -\Delta_2 \\ -\Delta_1 \end{pmatrix} \quad ; \quad n_{3,2} = \tfrac{1}{\ell}\begin{pmatrix} +\Delta_2 \\ -\Delta_1 \end{pmatrix}. \end{aligned} \tag{A4}$$

For a finite volume approach of the computation of the derivative, a direct use of formula (5) gives, integrating along the paths suggested in the figure,

$$\begin{aligned} \partial_1\phi &= \frac{1}{S}\Big(\frac{\ell}{2}\phi_1\Big(-\frac{\Delta_2}{\ell} - \frac{\Delta_2}{\ell}\Big) + \frac{\ell}{2}\phi_2\Big(\frac{\Delta_2}{\ell} + \frac{\Delta_2}{\ell}\Big) \\ &+ \frac{\ell}{2}\phi_3\Big(-\frac{\Delta_2}{\ell} + \frac{\Delta_2}{\ell}\Big) + \frac{\ell}{2}\phi_4\Big(\frac{\Delta_2}{\ell} - \frac{\Delta_2}{\ell}\Big)\Big) \\ &= \frac{1}{S}(-\phi_1\Delta_2 + \phi_2\Delta_2) \\ &= \frac{\phi_2 - \phi_1}{2\Delta_1}, \end{aligned} \tag{A5}$$

with a similar result for the second space direction. The results are

$$\partial_1\phi = \frac{\phi_2 - \phi_1}{2\Delta_1}, \tag{A6}$$

$$\partial_2\phi = \frac{\phi_4 - \phi_3}{2\Delta_2}. \tag{A7}$$

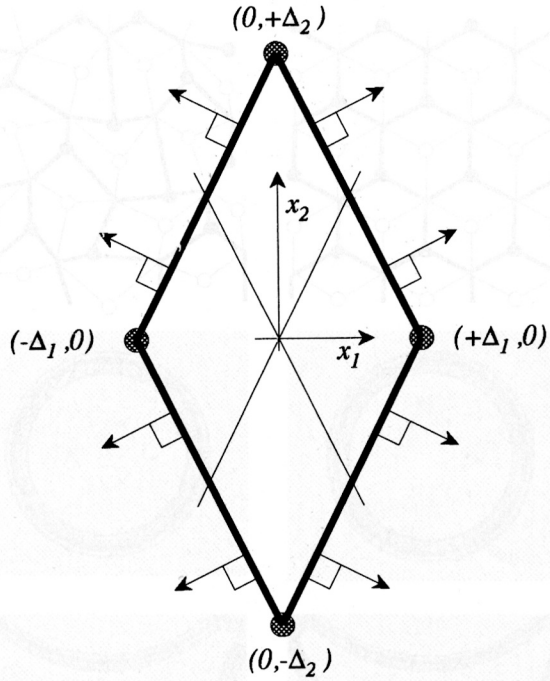

Figure 13. The lozenge, fundamental figure for 2-D finite volume computations in Cartesian grids.

A.2. Cartesian Grid, Three Dimensions

The basic element here is a rhombododecahedron. The formulas given here are for identical scaling along each axis ($\Delta_1 = \Delta_2 = \ldots = \Delta$), but it is easy to generalize. The coordinates of the six vertices used in the Cartesian grid are

$$\begin{aligned} P_1 &= (-\Delta, 0, 0), \\ P_2 &= (+\Delta, 0, 0), \\ P_3 &= (0, -\Delta, 0), \\ P_4 &= (0, +\Delta, 0), \\ P_5 &= (0, 0, -\Delta), \\ P_6 &= (0, 0, +\Delta). \end{aligned} \tag{A8}$$

The coordinates of the eight other vertices are

$$\begin{aligned} P_7 &= (+\Delta/2, +\Delta/2, +\Delta/2), \\ P_8 &= (-\Delta/2, -\Delta/2, +\Delta/2), \\ P_9 &= (+\Delta/2, -\Delta/2, -\Delta/2), \\ P_{10} &= (-\Delta/2, +\Delta/2, -\Delta/2), \\ P_{11} &= (+\Delta/2, -\Delta/2, +\Delta/2), \\ P_{12} &= (-\Delta/2, +\Delta/2, +\Delta/2), \\ P_{13} &= (+\Delta/2, +\Delta/2, -\Delta/2), \\ P_{14} &= (-\Delta/2, -\Delta/2, -\Delta/2). \end{aligned} \tag{A9}$$

The surface of the facets is given by

$$S = \frac{\Delta^2}{\sqrt{2}}. \tag{A10}$$

The volume is given by

$$V = 2\Delta^3. \tag{A11}$$

The 12 normals are

$$n_1 = \frac{1}{\sqrt{2}} \begin{pmatrix} +1 \\ +1 \\ 0 \end{pmatrix} \quad ; \quad n_2 = \frac{1}{\sqrt{2}} \begin{pmatrix} +1 \\ -1 \\ 0 \end{pmatrix} \quad ;$$

$$n_3 = \frac{1}{\sqrt{2}} \begin{pmatrix} -1 \\ +1 \\ 0 \end{pmatrix} \quad ; \quad n_4 = \frac{1}{\sqrt{2}} \begin{pmatrix} -1 \\ -1 \\ 0 \end{pmatrix} \quad ;$$

$$n_5 = \frac{1}{\sqrt{2}} \begin{pmatrix} +1 \\ 0 \\ +1 \end{pmatrix} \quad ; \quad n_6 = \frac{1}{\sqrt{2}} \begin{pmatrix} +1 \\ 0 \\ -1 \end{pmatrix} \quad ;$$

$$n_7 = \frac{1}{\sqrt{2}} \begin{pmatrix} -1 \\ 0 \\ +1 \end{pmatrix} \quad ; \quad n_8 = \frac{1}{\sqrt{2}} \begin{pmatrix} -1 \\ 0 \\ -1 \end{pmatrix} \quad ;$$

$$n_9 = \frac{1}{\sqrt{2}} \begin{pmatrix} 0 \\ +1 \\ +1 \end{pmatrix} \quad ; \quad n_{10} = \frac{1}{\sqrt{2}} \begin{pmatrix} 0 \\ +1 \\ -1 \end{pmatrix} \quad ;$$

$$n_{11} = \frac{1}{\sqrt{2}} \begin{pmatrix} 0 \\ -1 \\ +1 \end{pmatrix} \quad ; \quad n_{12} = \frac{1}{\sqrt{2}} \begin{pmatrix} 0 \\ -1 \\ -1 \end{pmatrix} . \tag{A12}$$

We now proceed to computation of the derivatives. Here, each value of the function whose derivatives are to be evaluated is given in each of the vertices having four adjacent facets, and the integration is made on the half of each of the facets adjacent to the vertex considered (see Figure 14). When directly using formula (6) only two values do not cancel, giving

$$V\,\partial_1\phi = -4\phi_1\left(\frac{\sqrt{2}}{2}\frac{\sqrt{2}}{4}\Delta^2\right) + 4\phi_2\left(\frac{\sqrt{2}}{2}\frac{\sqrt{2}}{4}\Delta^2\right), \tag{A13}$$

i.e.,

$$\partial_1\phi = \frac{\phi_2 - \phi_1}{2\Delta}, \tag{A14}$$

with similar results for the other two space dimensions. The results are

$$\partial_1\phi = \frac{\phi_2 - \phi_1}{2\Delta}, \tag{A15}$$

$$\partial_2\phi = \frac{\phi_4 - \phi_3}{2\Delta}, \tag{A16}$$

$$\partial_3\phi = \frac{\phi_6 - \phi_5}{2\Delta}. \tag{A17}$$

Appendix B: Formulas for minimal grids

B.1. Minimal Grid, Two Dimensions

The basic element here is a hexagon, of side Δ (see Figure 15).

The coordinates of the vertices are

$$\begin{aligned} P_1 &= (\ 0\ ,\ 0\ ), \\ P_2 &= (\ \Delta\ ,\ 0\ ), \\ P_3 &= (\ \tfrac{1}{2}\Delta\ ,\ \tfrac{\sqrt{3}}{2}\Delta\ ). \end{aligned} \tag{B1}$$

The length of the sides is

$$\ell = \frac{\Delta}{\sqrt{3}}. \tag{B2}$$

The surface is given by

$$S = \frac{\sqrt{3}}{2}\Delta^2. \tag{B3}$$

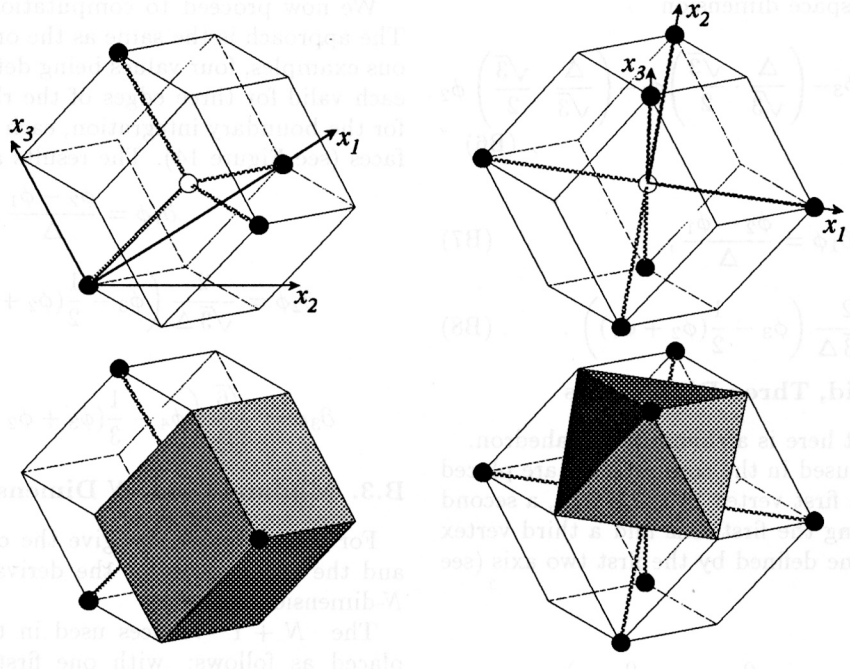

Figure 14. The rhombododecahedron is the central figure for both (left) minimal grids and (right) Cartesian grids. We show the location of axes and the surfaces of integration around each given value of the function.

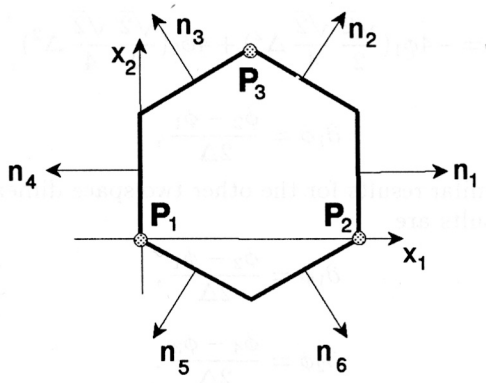

Figure 15. The hexagon, fundamental figure for 2-D finite volume computations in minimal grids.

The six normals are

$$n_1 = \begin{pmatrix} +1 \\ 0 \end{pmatrix} \quad ; \quad n_2 = \tfrac{1}{2}\begin{pmatrix} 1 \\ \sqrt{3} \end{pmatrix} \; ;$$

$$n_3 = \tfrac{1}{2}\begin{pmatrix} -1 \\ \sqrt{3} \end{pmatrix} \quad ; \quad n_4 = \begin{pmatrix} -1 \\ 0 \end{pmatrix} \; ; \tag{B4}$$

$$n_5 = \tfrac{1}{2}\begin{pmatrix} -1 \\ -\sqrt{3} \end{pmatrix} \quad ; \quad n_6 = \tfrac{1}{2}\begin{pmatrix} 1 \\ -\sqrt{3} \end{pmatrix} .$$

In computating the derivatives, a direct use of equation (4), with three values of the function being defined, valid each for two sides of the hexagon (see Figure 15), gives, for the first space dimension

$$S\,\partial_1\phi = \left(\frac{\Delta}{\sqrt{3}} + \frac{\Delta}{2\sqrt{3}}\right)\phi_2 - \left(\frac{\Delta}{\sqrt{3}} + \frac{\Delta}{2\sqrt{3}}\right)\phi_1 , \tag{B5}$$

and, for the second space dimension

$$S\,\partial_2\phi = \left(\frac{\Delta}{\sqrt{3}}\cdot\sqrt{3}\right)\phi_3 - \left(\frac{\Delta}{\sqrt{3}}\cdot\frac{\sqrt{3}}{2}\right)\phi_1 - \left(\frac{\Delta}{\sqrt{3}}\cdot\frac{\sqrt{3}}{2}\right)\phi_2 . \tag{B6}$$

The results are

$$\partial_1\phi = \frac{\phi_2 - \phi_1}{\Delta} , \tag{B7}$$

$$\partial_2\phi = \frac{2}{\sqrt{3}\,\Delta}\left(\phi_3 - \frac{1}{2}(\phi_2 + \phi_1)\right) . \tag{B8}$$

B.2. Minimal Grid, Three Dimensions

The basic element here is a rhombododecahedron.

The four vertices used in the computation are placed as follows: with one first vertex at the origin, a second vertex is placed along the first axis and a third vertex is placed on the plane defined by the first two axis (see Figure 14).

$$\begin{aligned} P_1 &= (\ 0 \ , \ 0 \ , \ 0 \ ), \\ P_2 &= (\ \Delta \ , \ 0 \ , \ 0 \ ), \\ P_3 &= (\ \tfrac{1}{2}\Delta \ , \ \tfrac{\sqrt{3}}{2}\Delta \ , \ 0 \ ), \\ P_4 &= (\ \tfrac{1}{2}\Delta \ , \ \tfrac{\sqrt{3}}{6}\Delta \ , \ \tfrac{\sqrt{6}}{3}\Delta \ ). \end{aligned} \tag{B9}$$

The surface of a facet is given by

$$S = \frac{\Delta^2}{2\sqrt{2}} . \tag{B10}$$

The volume is given by

$$V = \frac{\Delta^3}{\sqrt{2}} . \tag{B11}$$

The 12 normals are

$$n_1 = \tfrac{1}{\sqrt{3}}\begin{pmatrix} 0 \\ -1 \\ \sqrt{2} \end{pmatrix} \quad ; \quad n_2 = \tfrac{1}{2\sqrt{3}}\begin{pmatrix} \sqrt{3} \\ 1 \\ 2\sqrt{2} \end{pmatrix} \; ;$$

$$n_3 = \tfrac{1}{2\sqrt{3}}\begin{pmatrix} -\sqrt{3} \\ 1 \\ 2\sqrt{2} \end{pmatrix} \quad ; \quad n_4 = \begin{pmatrix} 1 \\ 0 \\ 0 \end{pmatrix} \; ;$$

$$n_5 = \tfrac{1}{2\sqrt{3}}\begin{pmatrix} \sqrt{3} \\ 3 \\ 0 \end{pmatrix} \quad ; \quad n_6 = \tfrac{1}{2\sqrt{3}}\begin{pmatrix} -\sqrt{3} \\ 3 \\ 0 \end{pmatrix} \; ;$$

$$n_7 = \begin{pmatrix} -1 \\ 0 \\ 0 \end{pmatrix} \quad ; \quad n_8 = \tfrac{1}{2\sqrt{3}}\begin{pmatrix} -\sqrt{3} \\ -3 \\ 0 \end{pmatrix} \; ;$$

$$n_9 = \tfrac{1}{2\sqrt{3}}\begin{pmatrix} \sqrt{3} \\ -3 \\ 0 \end{pmatrix} \quad ; \quad n_{10} = \tfrac{1}{2\sqrt{3}}\begin{pmatrix} \sqrt{3} \\ -1 \\ -2\sqrt{2} \end{pmatrix} \; ;$$

$$n_{11} = \tfrac{1}{2\sqrt{3}}\begin{pmatrix} -\sqrt{3} \\ -1 \\ -2\sqrt{2} \end{pmatrix} \quad ; \quad n_{12} = \tfrac{1}{\sqrt{3}}\begin{pmatrix} 0 \\ 1 \\ -\sqrt{2} \end{pmatrix} . \tag{B12}$$

We now proceed to computation of the derivatives. The approach is the same as the one shown with previous examples, four values being defined on four vertices each valid for three edges of the rhombododecahedron for the boundary integration, each being valid for three faces (see Figure 14). The results are

$$\partial_1\phi = \frac{\phi_2 - \phi_1}{\Delta} , \tag{B13}$$

$$\partial_2\phi = \frac{2}{\sqrt{3}\,\Delta}\left(\phi_3 - \frac{1}{2}(\phi_2 + \phi_1)\right) , \tag{B14}$$

$$\partial_3\phi = \frac{\sqrt{6}}{2\,\Delta}\left(\phi_4 - \frac{1}{3}(\phi_3 + \phi_2 + \phi_1)\right) . \tag{B15}$$

B.3. Minimal Grid, *N* Dimensions

For completeness, we give the coordinates of points and the expressions for the derivatives in the general N-dimensional case.

The $N + 1$ vertices used in the computation are placed as follows: with one first vertex at the origin, a second vertex is placed along the first axis, a third vertex is placed on the plane defined by the first two axes, a fourth vertex is placed on the hyperplane defined by the first three axes, and so on.

$$
\begin{array}{rcccccccc}
P_1 & = & (& 0 & , & 0 & , & 0 & , & 0 & , & \dots &) \\
P_2 & = & (& \frac{\sqrt{1}}{1}\Delta & , & 0 & , & 0 & , & 0 & , & \dots &) \\
P_3 & = & (& \frac{\sqrt{1}}{1\cdot 2}\Delta & , & \frac{\sqrt{1+2}}{2}\Delta & , & 0 & , & 0 & , & \dots &) \\
P_4 & = & (& \frac{\sqrt{1}}{1\cdot 2}\Delta & , & \frac{\sqrt{1+2}}{2\cdot 3}\Delta & , & \frac{\sqrt{1+2+3}}{3}\Delta & , & 0 & , & \dots &) \\
P_5 & = & (& \frac{\sqrt{1}}{1\cdot 2}\Delta & , & \frac{\sqrt{1+2}}{2\cdot 3}\Delta & , & \frac{\sqrt{1+2+3}}{3\cdot 4}\Delta & , & \frac{\sqrt{1+2+3+4}}{4}\Delta & , & \dots &) \\
\dots & = & (& \dots & , & \dots & , & \dots & , & \dots & , & \dots &) \\
P_{N+1} & = & (& \frac{\sqrt{1}}{1\cdot 2}\Delta & , & \frac{\sqrt{1+2}}{2\cdot 3}\Delta & , & \frac{\sqrt{1+2+3}}{3\cdot 4}\Delta & , & \dots & , & \frac{\sqrt{1+\dots+N}}{N}\Delta &) .
\end{array}
\tag{B16}
$$

The result is as follows:

$$
\partial_K \phi = \frac{1}{\Delta}\sqrt{\frac{2K}{K+1}}\left(\phi_{K+1} - \frac{1}{K}\sum_{i=1}^{K}\phi_i\right) . \tag{B17}
$$

Acknowledgments. The authors thank Claude Basdevant, Isabelle Faille, Thierry Gallouët and Jean-Paul Vila for very useful discussions. Work funded in part by the French Ministry of Superior Education and Research (MESR) through free access to the CM-5, and by the sponsors of the Geophysical Tomography Group (Amoco, CGG, DIA, Elf, IFP, Schlumberger, Statoil, and Total).

References

Edelsbrunner, H., *Algorithms in Combinatorial Geometry*, Springer-Verlag, New York, 1987.

Faille, I., T. Gallouët, and R. Herbin, Des mathématiciens découvrent les volumes finis, *Matapli (SMAI)*, *28*, 37–48, 1991.

Hermeline, F., Two coupled particle-finite volume methods using Delaunay-Voronoï meshes for the approximation of Vlasov-Poisson and Vlasov-Maxwell equations, *J. Comput. Phys.*, *106*, 1–18, 1993.

Kelly, K. R., R. W. Ward, S. Treitel, and R. M. Alford, Synthetic seismograms, a finite difference approach, *Geophysics*, *41*, 2–27, 1976.

Kittel, C., *Introduction to solid state physics*, John Wiley, New York, 1966.

Lax, P. D., and R. D. Richtmyer, Survey of the stability of linear finite difference equations, *Commun. Pure Appl. Math.*, *9*, 267–293, 1956.

Magnier, S.A., P. Mora, and A. Tarantola, Finite differences on minimal grids, *Geophysics*, *59*, 1435–1443, 1994.

Marfurt, K.J., Accuracy of finite-difference and finite-element modeling of the scalar and elastic wave equations, *Geophysics*, *49*, 533-549, 1984.

Virieux, J., P-SV wave propagation in heterogeneous media: Velocity-stress finite difference method, *Geophysics*, *51*, 889–901, 1986.

E. Dormy and A. Tarantola, Département de Sismologie, Institut de Physique du Globe de Paris, 4 place Jussieu, F-75252 Paris Cedex 05, France. (e-mail: dormy@ipgp.jussieu.fr and tarantola@ipgp.jussieu.fr)

(Received March 7, 1994; revised October 3, 1994; accepted October 6, 1994.)